13th International Symposium on Particle Image Velocimetry – ISPIV 2019
Munich, Germany, July 22-24, 2019

4D-PTV of inertial particles in two-way and four-way coupling regimes

Masoud Ebrahimian[1], R. Sean Sanders[2], Sina Ghaemi[1]*

[1] University of Alberta, Department of Mechanical Engineering, Edmonton, AB, Canada

[2] University of Alberta, Department of Chemical and Materials Engineering, Edmonton, AB, Canada

*ghaemi@ualberta.ca

Abstract

The effects of particle-turbulence and particle-particle interactions on dynamics of inertial particles were investigated in a non-isotropic turbulent channel flow. Experiments were carried out using glass beads with a mean diameter of 125 μm at volume concentrations of 0.03% (two-way coupling regime) and 0.15% (four-way coupling regime) in a horizontal channel flow operating at Reynolds numbers of Re_τ = 410 and 765, based on friction velocity and the channel half-height. The trajectory of particles was detected using time-resolved three-dimensional particle tracking velocimetry based on shake-the-box algorithm of Schanz et al. (2016). Results characterized the effect of particle-particle interaction on the particles acceleration statistics. Investigations illustrated that the extent of particle-particle interaction strongly depends on Re_τ.

1 Introduction

The prediction of particles motion in particle-laden turbulent flows is essential for improving the performance of industrial applications that include two-phase mixing/separation, combustion, and material transportation. In most of these applications the dynamics of transported particles deviates from the carrier phase due to their inertia. Hence, in investigation of particle-turbulence interaction (PTI), the particle dynamics is modeled using the particle's equation of motion, known as Maxey-Riley equation (Maxey and Riley, 1983; Bec et al., 2006; Lavezzo et al., 2010). In numerical investigations, particles are typically assumed as point-wise or smaller than Kolmogorov length scale and the flow velocity gradient around a particle is neglected. However, in real applications, particles are usually bigger than the Kolmogorov length scale, which can reduce the accuracy of the numerical investigations. On the other hand, the interaction of particles with each other can also affect their motion; but it is typically neglected in numerical investigations. Therefore, experimental investigations are still necessary to analyze the influence of particle-turbulence and particle-particle interactions on particles dynamics.

In previous studies, PTI has been described through three mechanisms including preferential sampling (Maxey, 1987), Basset mechanism (Basset, 1888), and inertial filtering (Bec et al., 2006). The effect of these mechanisms on particles motion has been typically characterized using particle Stokes number (St; the ratio of the particle relaxation time, t_p, to the flow time scale). This number represents a comparison of the particle inertia with the viscous force.

For inertial particles, the effect of inertial filtering mechanism on their motion becomes dominant compared with the preferential sampling and Basset mechanisms. The interaction of these particles with turbulence is highly affected by their inertia and they respond to a narrower range of eddy size (Bec et al., 2006; Ayyalasomayajula et al., 2008). Particles with large St typically have lower kinetic energy (Abrahamson, 1975) and lower acceleration (Ireland et al., 2016). Investigations of Zaichik

and Alipchenkov (2008) and Ireland et al. (2016) showed that acceleration variance reduces with increasing St.

The influence of particle-particle interaction (PPI) on particles motion has been typically characterized based on mass/volume concentration of particles (Elghobashi, 1994) in the flow and their relative velocity (Gourdel et al., 1999). Previous studies investigated the effect of PPI on the distribution of particles and their velocity statistics in turbulent flows. The results showed that the increment of PPI reduces the average particle number density close to the wall and increases it away from the wall (Varaksin et al., 2000; Kussin and Sommerfeld, 2002; Sommerfeld, 2003; Shokri et al., 2017). It also increases the particles' average streamwise velocity close to the wall and reduces it away from the wall (Laín et al., 2002; Lin and Chang, 2016; Li et al., 2016; Shokri et al., 2017). The reviewed literature shed light on the effect of PPI on particles distribution and velocity statistics in turbulent flows. However, in order to evaluate PPI in the equation of motion, particles acceleration needs to be investigated.

In this study, effects of PTI and PPI on particle dynamics are investigated experimentally in particle-laden turbulent flows. Measurements were carried out in two-way and four-way coupling regimes and at two different Re_τ. Particle trajectories were detected using a time resolved three-dimensional particle tracking velocimetry (3D-PTV) based on shake-the-box (STB) algorithm of Schanz et al. (2016). The trajectories of particles were used to determine their Lagrangian velocity and acceleration through a quadratic regression. The effect of PPI on the dynamics of inertial particles was investigated by comparing their velocity and acceleration statistics in two-way and four-way coupling regimes.

2 Experimental Setup

Experiments were carried out in a horizontal closed flow-loop that is showed in figure 1. The specifications of the unladen and two-phase experiments and the characteristics of the flow facility, inertial particles, and the 3D-PTV measurement system are described in the following sections.

2.1 Flow facility

The flow-loop had a 3 m long channel with a rectangular cross-section with the dimensions of (W×2H) = 120×15 mm^2, where W is the width of the channel and H is the channel half-height. Measurements were conducted at 220H downstream from the channel entrance to ensure a fully developed turbulent flow inside the test-section, which had glass walls for optical access. Two gradual transition sections were used at the two ends of the channel to connect it to the 2-inch diameter pipe sections. The flow was circulated inside the loop by a centrifugal pump (LCC-Metal, GIW Industries Inc.). A Coriolis flow meter (Micro Motion F-Series, Emerson Industries) with mass flow accuracy of 0.2% was used to measure the flow rate and the fluid temperature. A double-pipe heat exchanger was used to keep the temperature constant at 20°C during the experiments. The experiments were performed at two mass flow rates of 1.76 and 3.52 kg/s, corresponding to bulk velocity of U_b = 0.98 and 1.96 m/s across the channel, respectively. The unladen flow experiments were also carried out at similar Re_H of the particle-laden flows. The unladen flows were seeded by silver-coated tracers (SG02S40 Potters Industries) with 2 μm diameter and density of 3.6 g/cm^3. The properties of unladen experiments including the friction velocity, u_τ, inner length scale, λ, inner time-scale ($t_f = \upsilon/u_\tau^2$ where υ is the fluid kinematic viscosity), and $Re_\tau = u_\tau H/\upsilon$ are presented in table 1.

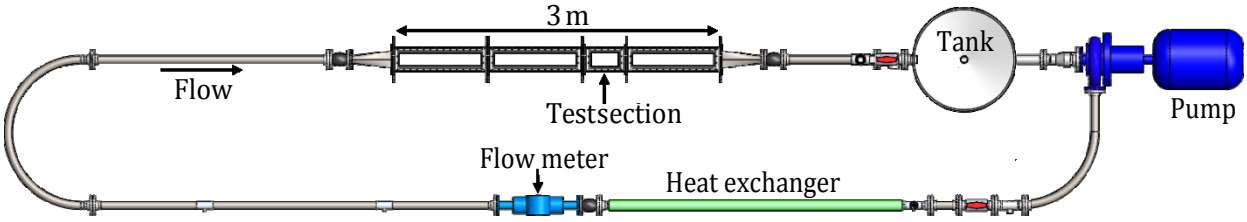

Figure 1: Top-view of the horizontal slurry flow-loop that was used for the present study. The flow-loop was equipped with a transparent test-section, a Coriolis flow meter, a centrifugal pump, and a heat exchanger to keep the temperature constant during the experiments.

Re_H	Re_τ	U_b, m/s	u_τ, m/s	λ, μm	t_f, ms
14,650	410	0.98	0.055	18	0.334
29,300	765	1.96	0.102	10	0.096

Table 1: Characteristics of the unladen turbulent flows tested in the present study. The inner scaling was determined based on the velocity profiles measured using 3D-PTV.

2.2 Particle-Laden flow

Glass beads with density of ρ_p = 2.5 g/cm^3 and mean diameter of d_p = 125 μm were used to perform the particle-laden experiments. The glass beads had terminal settling velocity of V_t = 0.013 m/s and Reynolds number, $Re_p = d_p V_t/\upsilon$, of 1.58. The beads' Stokes number was defined based on the inner time scale of the associated unladen flow experiment as $St_i = t_p/t_f$. The relaxation time of glass beads was about 1.28 ms that was calculated as $t_p = (\rho_p - \rho_f)d_p^2/(18\mu)f_d$, where ρ_f and μ are the fluid density and fluid dynamic viscosity, respectively. The drag correction factor of $f_d = 1+0.15Re_p^{0.687}$ was introduced by Clift and Gauvin (1971) to compensate the deviation from the Stokes' flow. The St_i of glass beads was 3.8 at Re_τ =410 and 13.3 at Re_τ =765. The glass beads were dispersed in water at volumetric concentrations of C_v = 0.03% and 0.15% that represent two-way and four-way coupling flow regimes, respectively (Elghobashi, 1994).

2.3 Time-resolved 3D-PTV

Measurements were performed using a time-resolved 3D-PTV system consisting of four Phantom v611 high-speed cameras (Vision Research Inc.) which were equipped with sigma SLR objective lenses with focal length of f = 105 mm. The lenses were set to an aperture size of $f/16$ and connected to cameras using Scheimpflug adapters. The cameras were positioned in a plus-like configuration, as shown in figure 2. The line-of-sight of each camera had a solid angle of about 35° from the y-axis. A high-speed controller (HSC v2, LaVision GmbH) commanded by DaVis 8.4 (LaVision GmbH) was used to synchronize the cameras with a dual-cavity Nd:YLF laser (DM20-527, Photonics Industries International Inc.). A collimator along with spherical and cylindrical lenses was used to change the laser beam to a laser sheet with cross section of 50×4 mm^2 in the streamwise (x) and wall-normal (y) directions. This laser sheet was directed into the test-section through the glass sidewall, passed the span of the test-section, flush to the bottom wall and exited from the opposite wall. A mirror was used after the test section, on the opposite side, to reflect the laser sheet back into the test-section and increase the light intensity. Two knife-edges were located outside the sidewalls to exactly limit the laser sheet in the region of $0 \le y \le 4$ mm. The center of the coordinate system was located at the

center of the bottom wall of the test section as shown in figure 2. The flow was in the positive *x* direction. The *y*-axis points in the wall-normal direction from the bottom wall toward the top wall, and the *z*-axis indicates the spanwise direction.

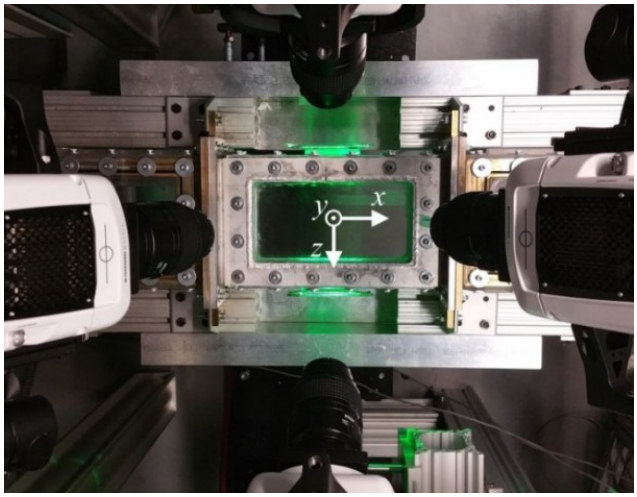

Figure 2: The top-view of the 3D-PTV setup, showing the test section and four high-speed cameras in a plus-like configuration. The collimator directs the laser sheet into the test section from side wall. A mirror was used on the other side of the test section to reflect the output laser sheet back into the test section and equalize the cameras' image intensity in backward and forward scattering orientations (Ghaemi and Scarano, 2010). The origin of the coordinate system is at the center of the bottom wall of the test section. The positive direction of the *y*-axis is toward the top wall.

A dual-plane calibration plate was used to project the physical coordinate system on the image coordinate system using a third order polynomial function. The mapping function showed that the 3D-PTV system had a magnification of 0.41 and a digital resolution of 0.049 mm/pixel. This magnification and aperture size resulted in the depth-of-focus of 7.9 mm. The resulted measurement volume is 50×4×30 mm^3. The mapping function was further improved using a volume self-calibration procedure at low seeding density to reduce the calibration errors (Wieneke, 2008). A volumetric optical transfer function was also determined for each camera to increase the accuracy of the 3D reconstruction procedure and reduce the number of ghost particles (Schanz et al., 2013;Schanz et al., 2016). The above processes were carried out in DaVis 8.4 (LaVision GmbH).

Image acquisition was carried out in single-frame mode using a cropped sensor size of 1024×608 pixel, and with simultaneous operation of both laser cavities in each frame. For unladen experiments, cameras were operated at an acquisition rate of 6 kHz for 3 seconds (three discrete sets of one-second image recording) at each Re_H. The acquisition rate of the imaging system was set on 10 kHz for particle-laden experiments to better resolve the glass beads motion in the vicinity of the wall. The particle-laden measurements were carried out for 5 seconds (five discrete sets of one-second image recording) at each Re_H. Silver-coated tracers and glass beads had a Gaussian intensity profiles with image diameter of approximately 3 pixels. Tracers had an average image number density of about 0.025 tracer per pixel in the unladen experiments. The maximum displacement of tracers at Re_τ of 410 and 765 of unladen experiments was about 4 and 8 pixels, respectively. The number density of the glass beads in the images at C_v of 0.03% and 0.15% were about 0.008 and

0.04 bead per pixel, respectively. Glass beads in particle-laden experiments had maximum displacement of about 3 and 5 pixels at Re_τ of 410 and 765, respectively.

The signal-to-noise ratio of the images was improved by subtracting the minimum intensity of the ensemble of images from each image, followed by subtraction of the local minimum intensity within a kernel of five pixels. The intensity of each pixel was also divided by the average intensity within a kernel of 50 pixels and the image intensity of all cameras' images was normalized relative to each other.

The 3D Lagrangian trajectories of tracers in unladen experiments and glass beads in particle-laden experiments were detected using STB algorithm (Schanz et al., 2016) carried out in DaVis 8.4 (LaVision, GmbH). In this process, the location of each tracer (or glass bead) was first estimated with an allowed triangulation error of 0.5 pixel (25 μm) in the images and then corrected by shaking the tracer/bead image within a kernel of 0.1 pixel in three dimensions. The maximum allowable displacement between two consecutive images was set to 6 and 9 pixels for tracers in unladen experiments for the low and high Re_τ cases, respectively. The maximum absolute change in the displacement of each tracer/bead between two consecutive time steps was set to 2 pixels with the maximum relative change of 10%. Table 2 shows the characteristics of the performed experiments including the number of the collected images (N_{im}), the approximate number of the detected trajectories by STB algorithm (N_{tr}), and the legend that is used to present their results in Section 3.

Experiment	Re_τ	C_v, %	$N_{im}\times10^{-3}$	$N_{tr}\times10^{-6}$	Legend
Unladen	410	-	27	9	LU
Particle-Laden	410	0.03	50	2	LL
Particle-Laden	410	0.15	50	3	LH
Unladen	765	-	27	10	HU
Particle-Laden	765	0.03	50	2	HL
Particle-Laden	765	0.15	50	3	HH

Table 2: The specifications of all the experiments that were performed in the present study.

The Lagrangian streamwise, wall-normal, and spanwise velocities (U, V, W) and accelerations (A_x, A_y, A_z) of each tracer/glass bead were determined by fitting a second order regression function on its trajectory. The optimal temporal kernel size of 4.5 ms for the experiments at Re_τ = 410 and 2 ms for the experiments at Re_τ = 765 was selected for the regression function, based on the root-mean-square (rms) of acceleration (Voth et al., 2002; Gerashchenko et al., 2008).

3 Results and discussion

3.1 Bead kinematics

To estimate the uncertainty of the 3D-PTV measurement system, the velocity statistics of unladen experiment at Re_τ = 410 are compared with DNS results of Moser et al. (1999) at Re_τ = 395 and its acceleration statistics are compared with DNS results of Yeo et al. (2010) at Re_τ = 408. The variation of $U^+ = \langle U\rangle/u_\tau$ (where $\langle\rangle$ is the ensemble average symbol over x, z, and time) for the unladen flows at low Re_τ (LU) and at high Re_τ (HU) with $y^+ = y/\lambda$ are presented in a semi-logarithmic profiles in figure 3(a) and compared with DNS results of Moser et al. (1999) at Re_τ = 395. The bin size for wall-normal averaging of the tracers in the unladen flow is equal to the corresponding λ. The linear viscous sublayer profile ($U^+ = y^+$) and the logarithmic law of the wall with κ = 0.4 and B = 5.2 are also

presented in this figure. The unladen measurements agree well with the DNS results from y^+ = 3.4 up to y^+ = 218 for LU and from y^+ = 6.2 up to y^+ = 400 for HU. This comparison shows the accuracy of the 3D-PTV measurements and also the fully developed state of the turbulent channel flows.

The mean streamwise velocity of glass beads is normalized with the friction velocity of the lower Re_τ ($u_{\tau 0}$) and presented in figure 3(b) as (U^+_0) along with the unladen counterparts. The wall-normal location, y, is normalized by the inner length scale of the lower Re_τ (λ_0) and presented as y^+_0 for all the profiles to compare the influence of PTI and PPI on glass beads motion at similar wall-normal location. The wall-normal averaging bin size for particle-laden results is d_p. At y^+_0 = 3.4, i.e. the first data point in the immediate vicinity of the lower channel wall, the U^+_0 of glass beads (U^+_{0p}) is higher than their unladen base (U^+_{0f}) in all particle-laden experiments since the no-slip boundary condition does not apply to the beads. The velocity difference between glass beads and their unladen base ($\Delta U^+_0 = |U^+_{0p} - U^+_{0f}|$) at this location is greater for the beads in four-way coupling regime than the beads in two-way coupling regime. This is due to PPI which increases the wall-normal momentum transfer of the beads and their velocity close to the wall (Laín et al., 2002; Shokri et al., 2017). In addition, for both two-way and four-way coupling regimes at the higher Re_τ, ΔU^+_0 at y^+_0 = 3.4 is larger. The greater St of the beads at the higher Re_τ increases inertial filtering of the particles and increases particles capability to maintain their streamwise momentum when they move toward the wall (Zhao et al., 2012). The increment of ΔU^+_0 by increasing Re_τ in four-way coupling regime is about 10% more than two-way coupling regime which is again due to the effect of PPI. Away from the wall, U^+_{0p} is less than U^+_{0f} for all experiments due to the higher inertia of beads than the fluid.

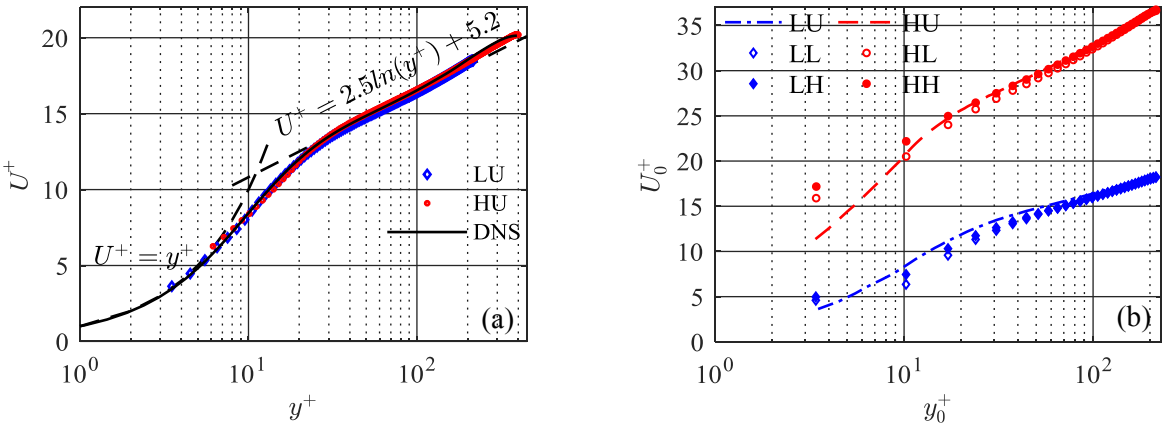

Figure 3: The wall-normal variation of normalized average streamwise velocity of (a) unladen flows and (b) glass beads in particle-laden flows. Legends are defined in table 2. The DNS result is from Moser et al. (1999) at Re_τ = 395.

3.2 Bead dynamics

The effects of PTI and PPI on acceleration statistics of particles are investigated in this section. The wall-normal variation of normalized mean acceleration in streamwise ($A^+_{x0} = \langle A_x \rangle \upsilon / u_{\tau 0}^3$) and wall-normal ($A^+_{y0}$) directions are presented in figure 4 for the unladen and the particle-laden experiments. Both A^+_{x0} and A^+_{y0} of unladen flow at Re_τ = 410 agree with the DNS results of Yeo et al. (2010) at Re_τ = 408 with maximum deviation of about 4% at y^+_0 = 8.6 for A^+_{x0} and about 2% at y^+_0 = 15.5 for A^+_{y0}. Due to the effect of viscous forces, the A^+_{x0} profiles of particle-laden experiments in figure 4(a) show deceleration of glass beads at y^+_0 < 20, similar to their unladen counterparts (Yeo

et al., 2010). The streamwise deceleration of inertial particles near the wall was also reported by Gerashchenko et al. (2008), Lavezzo et al. (2010), and Zamansky et al. (2011). With increasing C_v, the wall-normal migration of particles increases and more particles with high velocity move toward the wall. Although these particles increase U^+_{0p} in this region (see figure 3(b)), but their interaction with the high-shear region of the flow and other particles in the region decreases A^+_{x0} of particles close to the wall. Beyond the high-shear region of the flow at y^+_0>20, glass beads experience a positive A^+_{x0}, under the effect of streamwise pressure gradient of the flow. The increase of C_v also reduces A^+_{x0} of glass beads specifically at 20 < y^+_0 < 82. This region overlaps with the log-layer in low and high Re_τ. This is again due to the higher wall-normal migration of particles at higher C_v which increases the interaction of low-velocity and high-velocity glass beads in this region and lowers the effect of streamwise pressure gradient on their A^+_{x0}. The near wall data also shows that the effect of C_v on glass beads acceleration depends on Re_τ. For example, increasing C_v at low Re_τ, decreases A^+_{x0} of glass beads for about 40% at $y^+_0 \approx 31$, but this reduction at the same location is about 80% for the experiments at high Re_τ. This difference shows that the effect of PPI on the dynamics of particles depends on Re_τ and PTI. The increase of the bulk velocity also augments the viscous force near the wall by increasing the shear rate which increase deceleration of glass beads in this region.

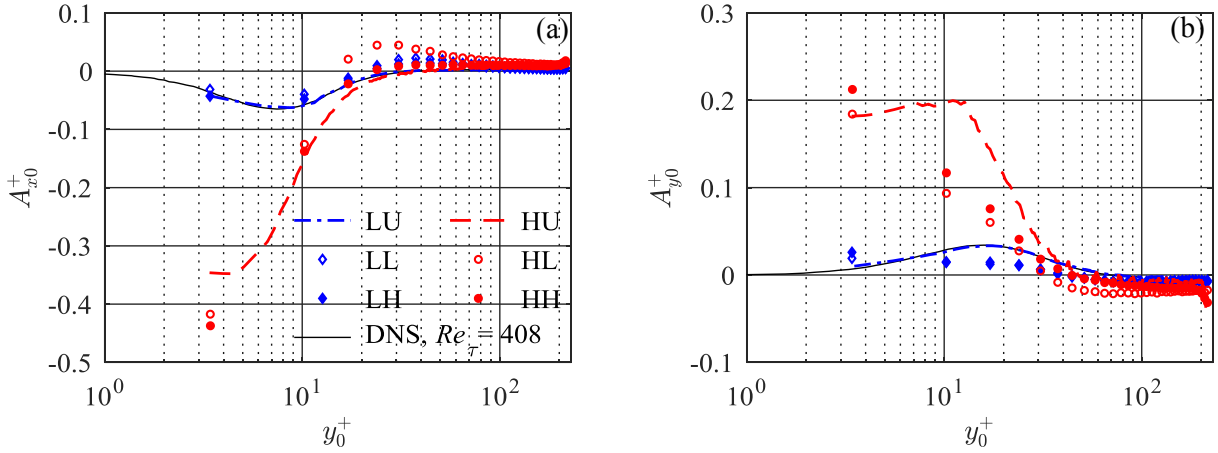

Figure 4: The wall-normal variation of (a) A^+_{x0} and (b) A^+_{y0} of unladen flows and the beads. Legends are defined in table 2. The solid lines show the DNS results of Yeo et al. (2010) at Re_τ = 408.

Figure 4(b) shows positive A^+_{y0} at y^+_0<40. The main source of positive A^+_{y0} for glass beads and their unladen counterparts in this region is the wall-normal pressure gradient of the quasi-streamwise vortices (Yeo et al., 2010). For downward moving beads, another factor that can provide positive A^+_{y0}, is the wall repulsive force due to the increase of pressure of the fluid layer between the wall and the beads approaching the wall (Feng et al., 1994). The third factor that can affect A^+_{y0} is the interaction of beads with each other. The collision of a downward moving bead with another glass bead applies an upward force to the first bead and pushes the other bead toward the wall. The motion of the latter toward the wall also causes wall repulsive force on it. Therefore, PPI which is intensified by increasing C_v, increases the A^+_{y0} of particles, particularly near the wall, as it is shown in figure 4(b). Further away from the wall, the effect of wall-normal pressure gradient and wall repulsive force on A^+_{y0} diminishes and the particles in that region experience a negative A^+_{y0} due to the gravity.

As it was shown in figure 4, PTI and PPI both affected the average acceleration of particles in the flow. The fluctuation of particles acceleration is also influenced by these two interactions. It is known that PTI is the main source of the intermittency of particles acceleration in particle-laden turbulent flows and its effect on particles is reduced by increasing St (Bec et al., 2006; Cencini et al., 2006). However, the effect of PPI on the acceleration fluctuation is still unknown. To address this issue, the rms of acceleration of particles in streamwise ($a^+_{x0} = \upsilon\langle A_x^2\rangle^{0.5}/u_{\tau 0}^3$), wall-normal ($a^+_{y0}$), and spanwise ($a^+_{z0}$) directions are investigated in two-way and four-way coupling regimes and results are presented in figure 5. Figure 5(a) shows that increasing C_v at the low Re_τ increases a^+_{x0} at $y^+_0 <$ 31 (e.g. for about 30% at $y^+_0 = 10.2$) due to the increase of local concentration of particles and the augmentation of PPI in this region. Away from the wall, however, increasing C_v does not have a significant effect on a^+_{x0}. At the higher Re_τ, increasing C_v does not affect a^+_{x0} near the wall significantly but it increases it away from the wall (e.g. for about 30% at $y^+_0 = 215$). At the higher Re_τ, increasing C_v increases the local concentration of particles away from the wall (Ahmadi et al., 2019) which increases the a^+_{x0} in that region. Therefore, result in figure 5(a) shows that PPI affects a^+_{x0} of particles and the extent of this effect depends on Re_τ.

The wall-normal variation of a^+_{y0} shows a stronger dependency on C_v than a^+_{x0}, as it is seen in figure 5(b). With increasing C_v, a^+_{y0} is increased in the whole measurement domain at the both Re_τ. The increment of wall-normal motion of particles at larger C_v increases the effect of PPI on their motion in this direction and increases a^+_{y0}. The increment of a^+_{y0} is larger close to the wall at the lower Re_τ and it is larger away from the wall for the higher Re_τ, again due to the effect of the local concentration of particles on PPI. Figure 5(c) shows that increasing C_v only has a negligible effect on a^+_{z0}.

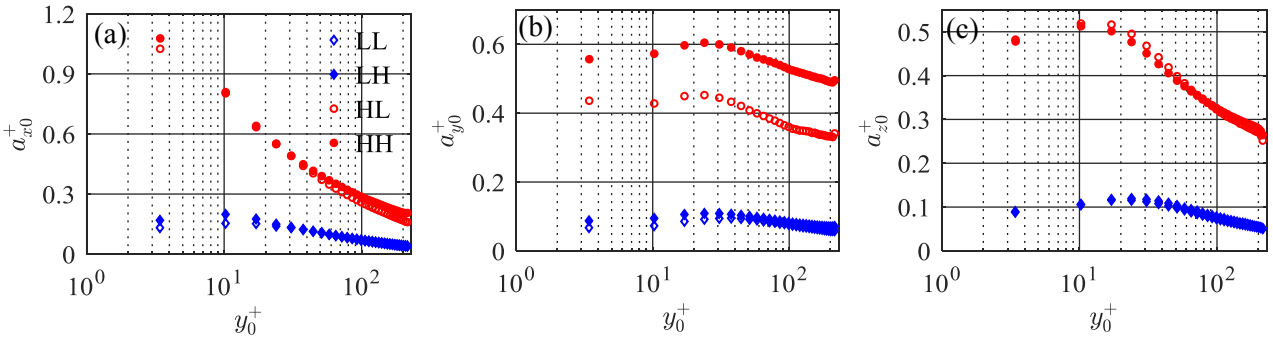

Figure 5: The wall-normal variation of (a) a^+_{x0}, (b) a^+_{y0}, and (c) a^+_{z0} of glass beads in particle-laden experiments. Legends are defined in table 2.

4 Summary and conclusion

The effect of PTI and PPI on the acceleration of inertial particles was investigated in particle-laden turbulent channel flows. Experiments were performed at Re_τ of 410 and 765, in two-way and four-way coupling regimes (at C_v = 0.03 and 0.15%, respectively) using 125 µm glass beads as the inertial particles. 3D-PTV measurement system was used based on the STB algorithm of Schanz et al. (2016) to detect the trajectory of particles. A quadratic regression was used to decrease the particle positioning noise and to determine the Lagrangian velocity and acceleration of particles. Results showed that increasing C_v reduces A^+_{x0} of particles close to the wall, and the effect of C_v on this deceleration depends on Re_τ. The A^+_{y0} of particles, however, increases particularly near the wall with

increasing C_v due to the effect of PPI on wall-normal motion of particles. The analysis particles acceleration rms showed that PPI can affect a^+_{x0} and particularly a^+_{y0}. The extent of this effect depended on Re_τ.

References

Abrahamson J (1975) Collision rates of small particles in a vigorously turbulent fluid. Chem. Eng. Sci. 30:1371–1379

Ahmadi F, Ebrahimian M, Sanders RS, and Ghaemi S (2019) Particle image and tracking velocimetry of solid-liquid turbulence in a horizontal channel flow. Int. J Multiphase Flow 112:83 –99

Ayyalasomayajula S, Warhaft Z, and Collins L (2008) Modeling inertial particle acceleration statistics in isotropic turbulence. Phys. Fluids 20:095104

Basset AB (1888) A treatise on hydrodynamics: with numerous examples. volume 2. Deighton, Bell and Company

Bec J, Biferale L, Boffetta G, Celani A, Cencini M, Lanotte A, Musacchio S, and Toschi F (2006) Acceleration statistics of heavy particles in turbulence. J Fluid Mech 550:349–358

Cencini M, Bec J, Biferale L, Boffetta G, Celani A, Lanotte A, Musacchio S, and Toschi F (2006) Dynamics and statistics of heavy particles in turbulent flows. J Turbul. page 36

Clift R and Gauvin W (1971) Motion of entrained particles in gas streams. The Canadian J of Chem. Eng. 49:439–448

Elghobashi S (1994) On predicting particle-laden turbulent flows. Appl Sci Res, 52:309–329

Feng J, Hu HH, and Joseph DD (1994) Direct simulation of initial value problems for the motion of solid bodies in a newtonian fluid. part 2. couette and poiseuille flows. J Fluid Mech 277:271–301

Gerashchenko S, Sharp N, Neuscamman S, and Warhaft Z (2008) Lagrangian measurements of inertial particle accelerations in a turbulent boundary layer. J Fluid Mech 617:255–281

Gourdel C, Simonin O, and Brunier E (1999) Two-Maxwellian equilibrium distribution function for the modelling of a binary mixture of particles. In Proceedings of the 6th Int Conference on Circulating Fluidized Beds. pages 205–210. DECHEMA, Frankfurt am Main, Germany

Ireland PJ, Bragg AD, and Collins LR (2016) The effect of Reynolds number on inertial particle dynamics in isotropic turbulence. Part 1. Simulations without gravitational effects. J Fluid Mech 796:617–658

Kussin J and Sommerfeld M (2002) Experimental studies on particle behavior and turbulence modification in horizontal channel flow with different wall roughness. Exp Fluids 33:143–159

Laín S, Sommerfeld M, and Kussin J (2002) Experimental studies and modelling of four-way coupling in particle-laden horizontal channel flow. Int J Heat Fluid Flow 23:647–656

Lavezzo V, Soldati A, Gerashchenko S, Warhaft Z, and Collins L (2010) On the role of gravity and shear on inertial particle accelerations in near-wall turbulence. J Fluid Mech 658:229–246

Maxey M (1987) The motion of small spherical particles in a cellular flow field. Phys Fluids 30:1915–1928

Maxey MR and Riley JJ (1983) Equation of motion for a small rigid sphere in a nonuniform flow. Phys Fluids 26:883–889

Moser RD, Kim J, and Mansour NN (1999) Direct numerical simulation of turbulent channel flow up to Re_τ= 590. Phys Fluids 11:943–945

Qureshi NM, Bourgoin M, Baudet C, Cartellier A, and Gagne Y (2007) Turbulent transport of material particles: an experimental study of finite size effects. Phys Rev lett 99:184502

Raffel M, Willert CE, Scarano F, Kaehler CJ, Wereley ST, and Kompenhans J (2018) Particle image velocimetry: a practical guide. Springer

Salazar JP and Collins LR (2012) Inertial particle relative velocity statistics in homogeneous isotropic turbulence. J Fluid Mech 696:45–66

Schanz D, Gesemann S, and Schroder A (2016) Shake-the-box: Lagrangian particle tracking at high particle image densities. Exp Fluids 57:70

Schanz D, Gesemann S, Schroder A, Wieneke B, and Novara M (2013) Non-uniform optical transfer functions in particle imaging: calibration and application to tomographic reconstruction. Meas Sci Technol 24:024009

Shokri R, Ghaemi S, Nobes D, and Sanders R (2017) Investigation of particle-laden turbulent pipe flow at high-reynolds-number using particle image/tracking velocimetry (PIV/PTV). Int J Multiphase Flow 89:136–149

Sommerfeld M (2003) Analysis of collision effects for turbulent gas–particle flow in a horizontal channel: Part I. particle transport. Int J Multiphase Flow 29:675–699

Varaksin AY, Polezhaev YV, and Polyakov AF (2000) Effect of particle concentration on fluctuating velocity of the disperse phase for turbulent pipe flow. Int J Heat Fluid Flow 21:562–567

Voth GA, la Porta A, Crawford AM, Alexander J, and Bodenschatz E (2002) Measurement of particle accelerations in fully developed turbulence. J Fluid Mech 469:121–160

Wieneke B (2008) Volume self-calibration for 3d particle image velocimetry. Exp Fluids 45:549–556

Yeo K, Kim BG, and Lee C (2010) On the near-wall characteristics of acceleration in turbulence. J Fluid Mech 659:405–419

Zaichik LI and Alipchenkov VM (2008) Acceleration of heavy particles in isotropic turbulence. Int J Multiphase Flow 34:865–868

Zamansky R, Vinkovic I, and Gorokhovski M (2011) Acceleration statistics of solid particles in turbulent channel flow. Phys Fluids 23:113304

Zhao L, Marchioli C, and Andersson H (2012) Stokes number effects on particle slip velocity in wall bounded turbulence and implications for dispersion models. Phys Fluids 24:021705